LETTERS
PUBLISHED ONLINE: 7 DECEMBER 2008 | DOI: 10.1038/NPHYS1152
nature physics

Long-lived quantum memory

R. Zhao[1], Y. O. Dudin[1], S. D. Jenkins[1,2]*, C. J. Campbell[1], D. N. Matsukevich[3], T. A. B. Kennedy[1] and A. Kuzmich[1]

Quantum memories for the storage and retrieval of quantum information are extremely sensitive to environmental influences, which limits their storage times. The ground states of atoms and ions are potential candidates for quantum memories, but although coherence times of the order of a few seconds for atoms[1,2] and hundreds of seconds for ions[3–5] have been demonstrated, long-lived storage and retrieval of single quantum excitations remains an outstanding challenge. Here, we report a quantum memory using the magnetically insensitive clock transition in atomic rubidium confined in a one-dimensional optical lattice. We observe quantum memory lifetimes exceeding 6 ms, more than two orders of magnitude longer than previously reported[6]. This advance is an important step towards the realization of long-distance quantum networks and the controlled production of complex entangled states of matter and light.

Protocols for quantum communication are typically based on remote parties sharing and storing an entangled quantum state. The generation of such remote entanglement must necessarily be done locally and distributed by light transmission over optical fibre links or through free space[7]. For the distribution of entanglement over a length L, the characteristic timescale for storage is the light travel time L/c, where c is the speed of light in the medium. For $L = 1{,}000$ km, $L/c \approx 5$ ms for an optical fibre.

In practice, direct entanglement distribution over optical fibres is limited by absorption to distances $l \sim 100$ km. To distribute entanglement over longer distances, the channel should be divided into links of length $\leq l$. The division circumvents attenuation in the fibre provided the intermediate memory nodes, which terminate the links, have a non-zero quantum memory time. Entanglement distributed over these shorter links is then connected over length L according to a family of protocols generically known as the quantum repeater[8]. The entanglement distribution rate of a network depends critically on the memory time of these storage elements. For $L \sim 1{,}000$ km, required memory times vary from many seconds for a simple network topology[8,9] to milliseconds for more complex (for example, multiplexed) topologies and architectures[10–12]. Such long-lived quantum memories could revolutionize deterministic single-photon sources[6] and lead to the generation of entangled states over extended systems[13].

Enhancing the matter coupling to a single spatial light mode is an advantage shared by cold optically thick atomic ensembles[14] and single atoms in high-finesse cavities[15]. The longest quantum memory time previously reported, 32 μs in a cold rubidium ensemble[6], is insufficient to carry out quantum repeater protocols over the distances where direct transmission fails. The rubidium sample, prepared in a state of zero average magnetization, was allowed to freely fall during the protocol and the quantum memory time was limited by the effects of small uncompensated magnetic fields. In short, equally populated atomic states of opposite magnetization, $\pm m\mu_B$, where m is the angular momentum projection and μ_B is the Bohr magneton, respond asymmetrically to ambient fields[16–23]. Ballistic expansion of the freely falling gas provides a longer memory time limitation, which can be estimated from the time $\tau = \Lambda/(2\pi v) \sim 100$ μs it takes an atomic spin grating to dephase by atomic motion (we use some representative parameters typical of the magneto-optical trap (MOT) environment: grating wavelength $\Lambda = 50$ μm, atomic velocity $v = \sqrt{k_B T/M} \simeq 8\,\mathrm{cm\,s^{-1}}$ for $T = 70$ μK and rubidium mass M). Millisecond storage of classical, coherent light has been reported in atomic gases[24–26], whereas coherence times in excess of 1 s have been achieved in the solid state[27].

To demonstrate quantum memory lifetimes of many milliseconds, we must suppress atomic motion and use magnetically insensitive atomic coherence as the basis of the quantum memory. Here, we report achieving this goal by confining rubidium-87 atoms in an optical lattice of 25 μm period using the $m = 0 \leftrightarrow 0$ ground-state atomic hyperfine transition for storage. We thereby take advantage of the magnetic insensitivity of the so-called clock transition, the energy of which depends only quadratically on the magnetic field strength. The ground hyperfine levels a and b of ^{87}Rb have angular momenta $F_a = 1$ and $F_b = 2$, and the upper and lower clock states are written as $|+\rangle \equiv |b, m = 0\rangle$ and $|-\rangle \equiv |a, m = 0\rangle$, respectively. If the atoms are prepared in the upper clock state by optical pumping, the $|+\rangle$ and $|-\rangle$ states can be coupled by Raman scattering of a weak linearly polarized write laser field into an orthogonally polarized signal field detected in the near-forward direction (Fig. 1).

The detection of the signal photon implies a momentum change $\hbar(\mathbf{k_w} - \mathbf{k_s})$ of the atoms (along the x' axis), where $\mathbf{k_w}$ and $\mathbf{k_s}$ are the write and signal field wave vectors, respectively. The excitation amplitude for an atom at position $\mathbf{r_\mu}$ is proportional to $e^{-i(\mathbf{k_w}-\mathbf{k_s})\cdot\mathbf{r_\mu}}$. The collective atomic excitation, imprinted with this phase grating, is the write spin wave. The spin wave coherence is essential in providing efficient coupling to a single spatial electromagnetic field mode in the retrieval stage, or read process, carried out after a controllable storage period. Optical confinement preserves the spin wave coherence by suppressing atomic motion along the $\mathbf{k_w} - \mathbf{k_s}$ direction.

The physics of the read process can be described using the concept of the clock polariton[28], a bosonic light–matter excitation with creation operator

$$\hat{\Psi}_0^\dagger(z,t) = \frac{\Omega\hat{\varphi}^\dagger(z,t) + i\kappa\sqrt{n}\hat{s}^\dagger(z,t)}{\sqrt{|\Omega|^2 + n|\kappa|^2}}. \qquad (1)$$

[1]School of Physics, Georgia Institute of Technology, Atlanta, Georgia 30332-0430, USA, [2]CNR-INFM, Dipartimento di Fisica e Matematica, Università degli Studi dell'Insubria, Via Valleggio 11 22100 Como, Italy, [3]Department of Physics, University of Maryland, College Park, Maryland 20742, USA.
*e-mail: stewart.jenkins@physics.gatech.edu.

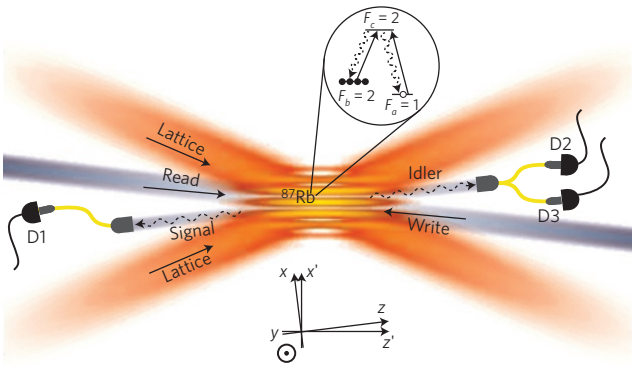

Figure 1 | Essential elements of the experimental set-up. Between 10^5 and 10^6 sub-Doppler-cooled ^{87}Rb atoms are loaded into an optical lattice (see the Methods section), and detection of the signal field, generated by Raman scattering of the write laser pulse (red-detuned by 20 MHz), heralds the presence of a write spin wave excitation. A resonant read/control field converts the surviving atomic excitation into an idler field after a storage period T_s. The inset shows the atomic level scheme of ^{87}Rb with levels a and b being the hyperfine components of the ground $5S_{1/2}$ level, and level c being a hyperfine component of the excited $5P_{1/2}$ level. The write laser excites the $b \leftrightarrow c$ transition, with Raman emission of the signal field on $c \rightarrow a$. The read laser excites the $a \leftrightarrow c$ transition, with Raman emission of the idler field on $c \rightarrow b$.

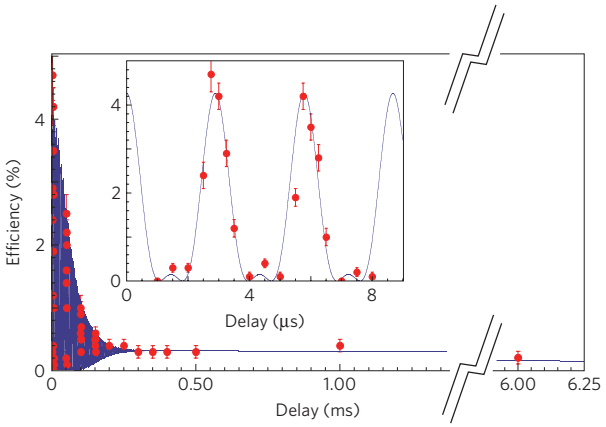

Figure 2 | Retrieval efficiency as a function of storage time: unpolarized atoms in an optical lattice. Experimental data, circles, show rapid damped oscillations due to Larmor precession at short times followed by slow decay on the millisecond timescale associated with the clock transition dephasing. The inset shows details of the short-time damped oscillations. The solid curves are fits based on the theory (see the Methods section). The observed 350 kHz oscillation frequency corresponds to $B_0 \approx 0.25$ G. Error bars represent ±1 standard deviation based on photoelectron counting statistics.

This is a linear combination of the read spin wave associated with the clock transition and the idler field propagating along the quantization axis z, and linearly polarized in the x direction; these are described by creation operators $\hat{s}^\dagger$ and $\hat{\varphi}^\dagger$, respectively. The form of the polariton operator shows that adiabatic variation of the y-polarized read field Rabi frequency Ω causes reversible conversion between the propagating idler field and the read spin wave. The collective Rabi frequency associated with the idler transition $c \rightarrow b$ is given by $\kappa\sqrt{n}$, where κ is the dipole coupling strength and n is the atomic number density.

Our goal is to convert the write spin wave, heralded by signal photodetection, into the idler field, with high efficiency. It is therefore essential to have a large overlap between the write and read spin waves. To maximize this overlap, the signal and idler spatial mode functions should be matched and the condition $\mathbf{k_i} = \mathbf{k_w} - \mathbf{k_s} + \mathbf{k_r}$ satisfied[29], where $\mathbf{k_i}$ and $\mathbf{k_r}$ are wave vectors for the idler and read fields, respectively. The overlap is also influenced by the atomic state preparation, angular momentum quantum numbers and transition strengths of the atomic levels a, b and c. For $F_a = 1, F_b = F_c = 2$ with atoms prepared in the $|+\rangle$ (upper clock) state, the write and read spin wave operators are equal, implying maximum efficiency.

As noted earlier, ballistic expansion limits the quantum memory time, and to increase it into the millisecond regime we load the atoms into a one-dimensional optical lattice as shown in Fig. 1. The period of the lattice 25 μm is shorter than the spin grating wavelength $\Lambda \simeq \lambda/\theta \approx 50\,\mu$m, determined by the angle $\theta \approx 0.9°$ between the write and signal fields of wavelength $\lambda = 795$ nm.

We outline in the Methods section the experimental procedure used to determine the retrieval efficiency and to demonstrate the quantum character of the memory through the α-parameter[30]. In Fig. 2, we show the retrieval efficiency as a function of storage time for an unpolarized atomic sample loaded into the lattice. We observe fast oscillations in the first two hundred microseconds followed by a slow decay on the scale of several milliseconds. The oscillations are caused by Larmor precession of magnetic hyperfine coherences of the write spin wave. A superposition of the states $|b, m\rangle$ and $|a, m'\rangle$ (hereafter referred to as $m \leftrightarrow m'$ coherence) precesses at a frequency $\omega_{m,m'} = (\mu_B B_0/\hbar)[g_a(m'+m) - \delta g m]$, where the Landé factors $g_a \approx -0.5018$, $g_b \approx 0.4998$ and $\delta g \equiv g_a + g_b = -0.002$; B_0 is the magnetic field. We note that because $\omega_{1,-1} \propto \delta g$, it is about 500 times smaller than $\omega_{1,1} \approx \omega_{2,0}$. The inset to Fig. 2 shows that the fast oscillations, associated with the $2 \leftrightarrow 0$ and $1 \leftrightarrow 1$ coherences, have a period of 2.8 μs corresponding to $B_0 \approx 0.25$ G. The expected 1.4 ms period oscillation of the slow $1 \leftrightarrow -1$ magnetic coherence, which has a small transition weight for this configuration, is not visible for this field. We have, however, observed this modulation by increasing the magnetic field to 2 G. The $0 \leftrightarrow 0$ coherence of the clock transition survives the decay of the magnetic coherences to a storage time of 6 ms (with a small contribution from the $1 \leftrightarrow -1$ coherence). The solid lines are fits to the data from the theory discussed in the Methods section, where the frequencies and decay times are treated as adjustable parameters. The ratio of maximum efficiency at short times to the efficiency at times longer than 200 μs is predicted, in the absence of atomic motion, to be $(32/13)^2 \approx 6.1$, whereas the observed value is approximately 13. As we discuss further below, the effects of atomic motion result in an extra dephasing of the spin wave, which may account for this observation. The asymptotic retrieval efficiency is clearly limited by the initial population $p_0 = 1/5$ of the clock state $|+\rangle$ in the unpolarized sample.

To further increase the efficiency at long times, we optically pump the atoms into the $|+\rangle$ state (see the Methods section). In this situation, much higher retrieval efficiencies at long storage times are observed. We note, however, that optical pumping results in a reduction of overall atomic number by a factor of 2–3, which must be accounted for when comparing the relative efficiencies. In Fig. 3a, two sets of data are shown, corresponding to maximum trap depths $U_0 = 40\,\mu$K and $U_0 = 80\,\mu$K, respectively, with a longer coherence time in the former case. All magnetic coherences are strongly suppressed by optical pumping, and, on the timescale shown, the fast magnetic coherences are completely dissipated, leaving primarily the clock hyperfine coherence. Atoms in the $|+\rangle$ and $|-\rangle$ clock states experience different, spatially varying light shifts in the lattice. The observed millisecond-scale decoherence of the clock spin wave may be attributed to the atomic motion in the lattice potential, accompanied by the phase broadening resulting from the differential light shifts[31]. Assuming a single harmonic trap, a formula for the decay of the clock

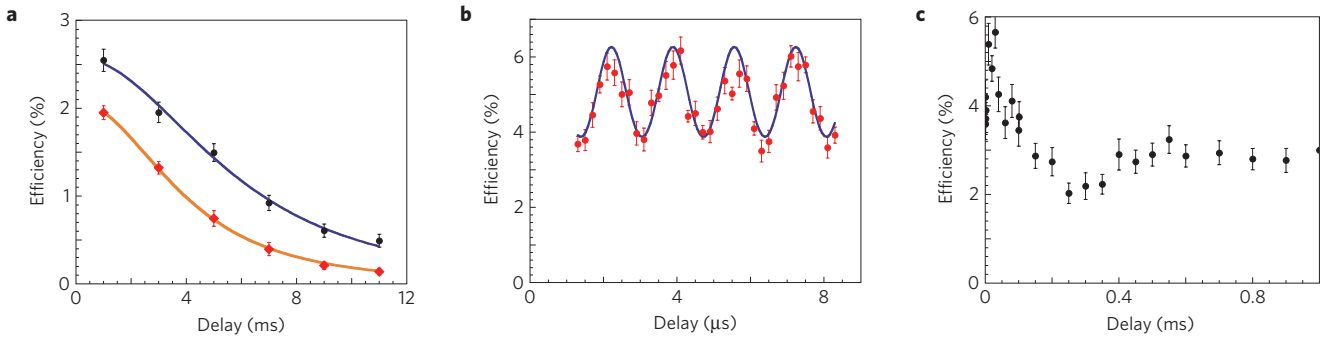

Figure 3 | Retrieval efficiency as a function of storage time for optically pumped atoms in an optical lattice. a, Diamonds, $U_0 = 80\,\mu$K; circles, $U_0 = 40\,\mu$K. The solid lines are fits of the form $(1+(t/T_c)^2)^{-3/2}$, with $T_c = 7.2 \pm 0.25$ ms (blue) and $T_c = 5.0 \pm 0.1$ ms (red)[31]. **b**, Short-time oscillations due to imperfect optical pumping. Experimental data, circles; solid line fit gives $B_0 = 0.43$ G and $p_0 \approx 0.85$ (see the Methods section), for $U_0 = 60\,\mu$K. **c**, Intermediate-time motional dephasing and damped oscillation, $U_0 = 60\,\mu$K. Error bars represent ±1 standard deviation based on photoelectron counting statistics.

transition coherence of the form $(1+(t/T_c)^2)^{-3/2}$ was derived[31]. Our lattice instead has a distribution of trap depths and the atoms do not necessarily perform simple harmonic motion. Within each well of the lattice the atoms are expected to be thermally distributed; however, they are not necessarily thermalized with respect to the global potential. Nevertheless, our data fit the formula well, and from this we extract the decay times $T_c \simeq (7, 5)$ ms for $U_0 \simeq (40, 80)\,\mu$K, respectively. According to the model of ref. 31, the decay time T_c corresponds to the (homogeneous lattice) equilibrium temperature $T = 2\hbar/(\xi k_B T_c)$, where ξ is the ratio of the ground-state hyperfine splitting to the effective detuning of the lattice light—here $\xi = 6.8 \times 10^{-5}$—resulting in values of $(30, 42)\,\mu$K.

In Fig. 3b, we show short-time dynamics for the optically pumped sample and, as expected, observe much lower visibility oscillations than those in Fig. 2. The data suggest the clock state $|+\rangle$ population $p_0 \approx 0.85$, and $p_{\pm 1} \approx 0.07$, assuming that $p_{\pm 2} \approx 0$. In Fig. 3c, optical pumping enables us to observe motional dephasing on the scale of a few hundred microseconds, followed by a damped evolution towards the 1 ms timescale, the efficiency dropping by about 50% (this typical behaviour is also to be expected in the data of Fig. 3a, but is not shown here). In common with Fig. 2, we attribute this fast dephasing to atomic oscillations along the lattice axis x'. A simple one-dimensional model of harmonic motion yields the characteristic behaviour shown in Fig. 3c if we average over a distribution of oscillator frequencies corresponding to a distribution of trap depths. We have also observed this qualitative behaviour in (3+1)-dimensional Monte Carlo simulations that include the full atomic orbits.

Having measured high retrieval efficiencies, we now demonstrate the quantum nature of the memory, on the 5 ms timescale. Specifically, we characterize how well the retrieved idler field compares to a single-photon state by measuring the α-parameter of Grangier *et al.*[30]. The value $\alpha = 0$ corresponds to an ideal, heralded single-photon state, whereas for classical fields $\alpha \geq 1$.

A field in a single-photon state incident on a beamsplitter is either transmitted or reflected, and the joint photoelectric detection probability vanishes. As described in the Methods section, we determine α from the measured set of joint photoelectric detection probabilities on the three detectors, D1–3, Fig. 1. It is important to appreciate that α is weakly dependent on retrieval efficiency until the idler field background becomes significant[16], and for this reason we do not expect α to significantly increase with storage time under the conditions of our experiment. Accounting for the measured signal field detection probability and efficiency, and idler channel background contribution, we theoretically estimate $\alpha \approx 0.02$ for 1.2 μs delay and $\alpha \sim 0.05$–0.1 for longer delays. In Table 1, we give the measured values of α, the main results of this paper, demonstrating quantum memory for storage times up to 6 ms. We have verified that detection of classical light with our protocol gives $\alpha = 0.97 \pm 0.08$, consistent with unity. Also shown in Table 1 are the corresponding values of the measured and intrinsic retrieval efficiencies obtained from the same data runs as the α-parameter (see the Methods section). We note that the short time measured (6.3%) and intrinsic (25%) retrieval efficiencies are smaller than our previous values of 7.5% and 34%, respectively[6], owing to the difficulty of spatially matching the lattice-loaded atomic sample and the signal–idler modes.

Table 1 | Measured values of α, measured efficiency η and intrinsic efficiency η_{int} (see the Methods section).

T (ms)	α	η (%)	η_{int} (%)
0.0012	0.02±0.01	6.3	25
1	0.12±0.04	2.8	11
4	0.17±0.07	1.3	5
6	0.10±0.10	1.1	4.5

Table 2 | Measured values of $g_D^{(2)}(0)$, measured deterministic single-photon source efficiency ϵ and intrinsic source efficiency ϵ_{int} (see the Methods section).

t_p (ms)	$g_D^{(2)}(0)$	ϵ (%)	ϵ_{int} (%)
4	0.06±0.04	1.9	8
5	0±0.06	1.6	6

An important, immediate application of this long quantum memory is the realization of a deterministic single-photon source based on quantum measurement and feedback, as proposed in ref. 6. There, the source was implemented using a freely expanding atomic cloud, with a quantum memory time of 32 μs, and two-photon events were reduced to 40% of the coherent state value[6]. As the protocol's success is based on long memory times, we are now able to significantly improve the quality of the single-photon source. The procedure closely resembles that used to measure retrieval efficiencies and α, with the following important distinction: instead of waiting for a period T_s after the signal detection event, we decide to read out the idler at time t_p. Hence, we begin the quantum feedback protocol at time $t_p - T_s$ (see the Methods section).

The quality of a deterministic single-photon source is demonstrated by measuring sub-Poissonian photoelectron statistics of the second-order coherence function $0 \le g_D^{(2)}(0) < 1$. The source efficiency, defined as the probability ϵ to detect a photoelectric event per trial, is the second important figure of merit. Ideally, $g_D^{(2)}(0) = 0$ and $\epsilon = 1$. The measured values of $g_D^{(2)}(0)$ and ϵ are given in Table 2. The former are comparable to those recently achieved using a single trapped atom in a high-finesse cavity, whereas our measured efficiencies are about a factor of two greater[15].

Methods

Retrieval efficiency. A write process using a detuned laser field creates an excitation in the atomic ensemble as illustrated in Fig. 1, resulting in the emission of a signal photon as an atom is transferred between levels b and a.

Under the phase-matching conditions discussed in the text, the read spin wave takes the form[29]

$$\hat{S}(t) = \int \mathrm{d}z\, \sqrt{f(z)}\hat{s}(z,t),$$

where $f(z) \equiv n(z)/\int \mathrm{d}z\, n(z)$. The corresponding clock polariton operator is given by

$$\hat{\Upsilon}(t) = \int \mathrm{d}z\ \sqrt{f(z)}\,\hat{\Psi}_0(z,t),$$

and these are identical in the absence of the control field, $\Omega = 0$, equation (1). To calculate the retrieved idler field efficiency, we evaluate the average number of polaritons stored at time T_s after detection of the signal photon, $N_\Upsilon(T_s) \equiv \langle \hat{\Upsilon}^\dagger(T_s)\,\hat{\Upsilon}(T_s)\rangle = \mathrm{Tr}\,(\hat{\rho}\,\hat{\Upsilon}^\dagger(T_s)\,\hat{\Upsilon}(T_s))$.

Conditioned on the detection of a signal photon, the collective atomic state is given by the density operator[6]

$$\hat{\rho} = \frac{1}{p_s}\sum_{n=1}^{\infty}\frac{\tanh^{2n}\chi}{\cosh^2\chi}\left(1-(1-\eta_s)^n\right)\frac{\hat{A}^{\dagger n}}{\sqrt{n!}}\hat{\rho}_0\frac{\hat{A}^n}{\sqrt{n!}},$$

where χ is the coupling strength, $\hat{A}, \hat{A}^\dagger$ are single-mode write spin wave annihilation and creation operators, η_s is the overall propagation and detection efficiency for the signal field and $p_s = \eta_s \sinh^2\chi/(1+\eta_s\sinh^2\chi) \ll 1$ is the probability of the signal photoelectric detection event per write pulse. For a perfectly optically pumped sample $\hat{\rho}_0 = \bigotimes_i |+\rangle_i\langle+|$, the operator $\hat{A} = \hat{S}(t=0)$.

It is straightforward to show that $N_\Upsilon(T_s) = |[\,\Upsilon(T_s), \hat{A}^\dagger]|^2\langle \hat{A}^\dagger\hat{A}\rangle$, so that the retrieved idler efficiency is given by

$$\eta_i(T_s) = \left|\left[\,\hat{\Upsilon}(T_s), \hat{A}^\dagger\right]\right|^2.$$

To assess the effects of an inhomogeneous magnetic field on the retrieval efficiency, we assume a magnetic field $\mathbf{B} = B_0\hat{z} + B'(z\hat{z} - \rho\hat{\rho}/2)$ and a Gaussian cloud density distribution of the form $f(z) = \exp\left(-z^2/2l^2\right)/\sqrt{2\pi l^2}$. We find

$$\eta_i(T_s) = \left|\int \mathrm{d}z\, f(z)\mathrm{e}^{-i\Delta\omega_0(z)T_s}\right|^2 = \mathrm{e}^{-T_s^2/\tau^2},$$

where $1/\tau = 4\pi\cdot 575\ [\mathrm{Hz\,G^{-2}}]\ B_0 B' l$ follows from the quadratic Zeeman shift $\Delta\omega_0(z)$ of the clock transition. Under the conditions of our experiment $B_0 = 0.5$ G, $B' \ll 100\ \mathrm{mG\,cm^{-1}}$, we find $\tau \gg 100$ ms.

The effects of the magnetic field on a partially polarized sample can be explained by generalizing the previous theoretical arguments to an N-atom mixed state of the form $\hat{\rho}_0 = \bigotimes_{\mu=1}^{N}\sum p_m |b,m\rangle_\mu\langle b,m|$, with $p_m = p_{-m}$. We find the retrieval efficiency

$$\eta_i(T_s) = \eta_0\left|p_0\mathrm{e}^{-\frac{T_s^2}{4\tau^2}} + \frac{p_1}{12}\mathrm{e}^{-\frac{T_s^2}{2\tau_{1,-1}^2}}\cos\left(\omega_{1,-1}T_s\right) + \frac{5p_1}{4}\mathrm{e}^{-\frac{T_s^2}{2\tau_{1,1}^2}}\cos\left(\omega_{1,1}T_s\right) + \frac{p_2}{3}\mathrm{e}^{-\frac{T_s^2}{2\tau_{2,0}^2}}\cos\left(\omega_{2,0}T_s\right)\right|^2,$$

where η_0 is the retrieval efficiency of an optically pumped sample at $T_s = 0$ and the numerical coefficients depend on $3j$ symbols; details will be given elsewhere. Furthermore, $\tau_{1,\pm1}$ and $\tau_{2,0}$ are decay times associated with the magnetic hyperfine coherences $|b,1\rangle \leftrightarrow |a,\pm1\rangle$ and $|b,2\rangle \leftrightarrow |a,0\rangle$. These are due to the linear Zeeman effect and are given by $\tau_{m,m'} = \hbar/(|g_a m' - g_b m|\mu_B \Delta B)$, where $\Delta B = B'l + \delta B$, and δB is a phenomenological width due to fast temporal variations of the magnetic field.

Experimental methods. The main elements of our experiment are shown in Fig. 1. A sample of ^{87}Rb atoms is collected and cooled in a MOT for a period of 0.2–0.5 s. Next, the trap laser is detuned to 90 MHz below atomic resonance and the repump laser intensity is lowered, for 20 ms, to optimize sub-Doppler cooling and lattice loading. The quadrupole coils of the MOT are switched off, and the bias field of 0.2–2 G, directed along the z axis, is switched on (the ambient magnetic field compensated by three pairs of Helmholtz coils). The optical lattice is made by interfering two beams of light at 1.06 μm, with power varying between 3.5 and 7 W per beam, and intersecting at an angle $\theta \approx 2.5°$. The waists of the two beams were ∼130 and ∼260 μm, respectively. The maximum lattice depth U_0 is varied between ∼40 (3.5 W per beam) and ∼80 (7 W per beam) μK. For the latter case, the corresponding (maximum) trap frequencies are $\approx 2.5\times10^3$, 110 and 2 Hz along the x', y and z' axis, respectively. We use optical pumping with light propagating along the x axis and linearly polarized along the z axis, resonant to the $b \leftrightarrow c$ transition. A repump laser resonant on the $a \leftrightarrow c$ transitions assists in the transfer of the atoms into the upper clock state $|+\rangle$.

The temperature of the cloud, which is strongly confined in the x'–y plane, was measured by ballistic expansion at an angle of 30° to the horizontal, and found to be (8, 17) μK for $U_0 \simeq (40, 80)$ μK, respectively. As might be expected, these differ significantly from the homogeneous lattice model discussed in the text. There are a number of extra mechanisms, such as misalignment of the lattice with respect to the spin wave, quadratic Zeeman (clock) shift, collisional broadening, laser pointing instability and spontaneous scattering of the lattice light, that we believe produce much smaller decoherence than differential light shifts.

The retrieval efficiency and α-parameter are measured using the following protocol. We carry out a sequence of trials; each trial begins with a write pulse and terminates with a clean pulse, which resets the atomic state, until the signal detector, D1, registers a photoelectric detection event. At this point, the sequence is terminated, and the prepared spin wave is stored for the time T_s, after which time a read pulse converts the excitation into an idler field, which is directed onto a beamsplitter followed by photodetectors D2 and D3.

The measured retrieval efficiency is determined by the sum of probabilities $p_2 + p_3$ to detect photoelectric events at D2 and D3, respectively. All of the measured retrieval efficiencies shown in Figs 2 and 3 are taken for the signal photodetection probability at detector D1, $p_1 \approx 5$–7×10^{-4}, whereas for the data in Table 1, $p_1 \approx 1.6$–4×10^{-4}. We have verified that all of the measured idler efficiencies are independent of p_1, so that they have negligible background contributions up to times longer than 7 ms.

The anticorrelation parameter α is given by the ratio of various onefold, twofold and threefold photoelectric detection probabilities measured by the set of detectors D1, D2 and D3 (ref. 30):

$$\alpha = \frac{p_1 p_{123}}{p_{12}p_{13}}.$$

The second-order coherence function $g_D^{(2)}$,

$$g_D^{(2)}(0) = p_{23}/(p_2 p_3),$$

quantifies the quality of single photons produced by the following quantum feedback protocol. Each trial begins with a write pulse. If D1 registers a signal photoelectric event, the protocol is halted. The memory is now armed with a spin wave excitation and is left undisturbed until the time t_p when a read pulse converts it into the idler field. If D1 does not register an event, the atomic memory is reset to its initial state with a cleaning pulse, and the trial is repeated. The duration of a single trial is 1 μs. If D1 does not register a signal detection event by $t_p - 49$ μs, the protocol is halted and any background counts in the idler channel are detected and included in the measurement record.

We have verified that for classical light our experimental protocol resulted in $g_D^{(2)}(0) = 0.99 \pm 0.05$. In this letter, the retrieval efficiencies η discussed are measured efficiencies, referring to photoelectric detection probabilities per read pulse. The uncertainties given are based on the statistics of photoelectron counting events. The measured passive losses from the atomic sample to the detector in the idler channel produce an efficiency factor of $0.25 \pm 10\%$. Intrinsic efficiencies η_{int} and ϵ_{int} are therefore greater than η and ϵ by a factor of 4, respectively, as shown in Tables 1 and 2.

Received 16 June 2008; accepted 10 November 2008; published online 7 December 2008

References

1. Harber, D. M., Lewandowski, H. J., McGuirk, J. M. & Cornell, E. A. Effect of cold collisions on spin coherence and resonance shifts in a magnetically trapped ultracold gas. *Phys. Rev. A* **66**, 053616 (2002).
2. Treutlein, P. *et al.* Coherence in microchip traps. *Phys. Rev. Lett.* **92**, 203005 (2004).
3. Bollinger, J. J. *et al.* A 303-MHz frequency standard based on trapped Be+ ions. *IEEE Trans. Instrum. Meas.* **40**, 126–128 (1991).
4. Langer, C. *et al.* Long-lived qubit memory using atomic ions. *Phys. Rev. Lett.* **95**, 060502 (2005).

5. Haffner, H. *et al.* Robust entanglement. *Appl. Phys. B* **81**, 151–153 (2005).
6. Matsukevich, D. N. *et al.* Deterministic single photons via conditional quantum evolution. *Phys. Rev. Lett.* **97**, 013601 (2006).
7. Aspelmeyer, M. *et al.* Long-distance free-space distribution of quantum entanglement. *Science* **301**, 621–623 (2003).
8. Briegel, H.-J., Duer, W., Cirac, J. I. & Zoller, P. Quantum repeaters: The role of imperfect local operations in quantum communication. *Phys. Rev. Lett.* **81**, 5932–5935 (1998).
9. Duan, L.-M., Lukin, M., Cirac, J. I. & Zoller, P. Long-distance quantum communication with atomic ensembles and linear optics. *Nature* **414**, 413–418 (2001).
10. Collins, O. A., Jenkins, S. D., Kuzmich, A. & Kennedy, T. A. B. Multiplexed memory-insensitive quantum repeaters. *Phys. Rev. Lett.* **98**, 060502 (2007).
11. Jiang, L., Taylor, J. M. & Lukin, M. D. Fast and robust approach to long-distance quantum communication with atomic ensembles. *Phys. Rev. A* **76**, 012301 (2007).
12. Sangouard, N. *et al.* Robust and efficient quantum repeaters with atomic ensembles and linear optics. *Phys. Rev. A* **77**, 062301 (2008).
13. Duan, L.-M. Entangling many atomic ensembles through laser manipulation. *Phys. Rev. Lett.* **88**, 170402 (2002).
14. Matsukevich, D. N. & Kuzmich, A. Quantum state transfer between matter and light. *Science* **306**, 663–666 (2004).
15. Hijlkema, M. *et al.* A single-photon server with just one atom. *Nature Phys.* **3**, 253–255 (2007).
16. Chanelière, T. *et al.* Storage and retrieval of single photons transmitted between remote quantum memories. *Nature* **438**, 833–836 (2005).
17. Matsukevich, D. N. *et al.* Observation of dark state polariton collapses and revivals. *Phys. Rev. Lett.* **96**, 033601 (2006).
18. Jenkins, S. D. *et al.* Theory of dark-state polariton collapses and revivals. *Phys. Rev. A* **73**, 021803(R) (2006).
19. Matsukevich, D. N. *et al.* Entanglement of remote atomic qubits. *Phys. Rev. Lett.* **96**, 030405 (2006).
20. Chen, Y. A. *et al.* Memory-built-in quantum teleportation with photonic and atomic qubits. *Nature Phys.* **4**, 103–107 (2007).
21. Simon, J., Tanji, H., Ghosh, S. & Vuletic, V. Single-photon bus connecting spin-wave quantum memories. *Nature Phys.* **3**, 765–769 (2007).
22. Laurat, J. *et al.* Heralded entanglement between atomic ensembles: Preparation, decoherence, and scaling. *Phys. Rev. Lett.* **99**, 180504 (2007).
23. Choi, K. S., Deng, H., Laurat, J. & Kimble, H. J. Mapping photonic entanglement into and out of a quantum memory. *Nature* **452**, 67–74 (2008).
24. Liu, C., Dutton, Z., Behroozi, C. H. & Hau, L. V. Observation of coherent optical information storage in an atomic medium using halted light pulses. *Nature* **409**, 490–493 (2001).
25. Phillips, D. F. *et al.* Storage of light in atomic vapor. *Phys. Rev. Lett.* **86**, 783–786 (2001).
26. Julsgaard, B. *et al.* Experimental demonstration of quantum memory for light. *Nature* **432**, 482–486 (2004).
27. Longdell, J. J., Fraval, E., Sellars, M. J. & Manson, N. B. Stopped light with storage times greater than one second using electromagnetically induced transparency in a solid. *Phys. Rev. Lett.* **95**, 063601 (2005).
28. Fleischhauer, M. & Lukin, M. D. Dark-state polaritons in electromagnetically induced transparency. *Phys. Rev. Lett.* **84**, 5094–5097 (2000).
29. Jenkins, S. D. *Theory of Light-Atomic Ensemble Interactions*. PhD thesis, Georgia Inst. Technology (2006).
30. Grangier, P., Roger, G. & Aspect, A. Experimental evidence for a photon anticorrelation effect on a beam splitter: A new light on single-photon interferences. *Europhys. Lett.* **1**, 173–179 (1986).
31. Kuhr, S. *et al.* Analysis of dephasing mechanisms in a standing-wave dipole trap. *Phys. Rev. A* **72**, 023406 (2005).

Acknowledgements

We thank P. Ahmadi, T. Chanelière, M. S. Chapman and S.-Y. Lan for discussions. This work was supported by the National Science Foundation, the A. P. Sloan Foundation and the Office of Naval Research.

Additional information

Reprints and permissions information is available online at http://npg.nature.com/reprintsandpermissions. Correspondence and requests for materials should be addressed to S.D.J.